1-12-2020

Analyses of the oncogenic BRAFD594G variant reveal a kinase-independent function of BRAF in activating MAPK signaling

Nicholas J. Cope

Borna Novak

Zhiwei Liu
liuz@rowan.edu

Amber Y. Gunderwala

Matthew Connolly

See next page for additional authors

Recommended Citation

Analyses of the oncogenic BRAFD594G variant reveal a kinase-independent function of BRAF in activating MAPK signaling Cope, Nicholas J. et al. Journal of Biological Chemistry, Volume 295, Issue 8, 2407 - 2420

Analyses of the oncogenic BRAF^{D594G} variant reveal a kinase-independent function of BRAF in activating MAPK signaling

Received for publication, October 19, 2019, and in revised form, January 7, 2020 Published, Papers in Press, January 12, 2020, DOI 10.1074/jbc.RA119.011536

Nicholas J. Cope, Borna Novak, Zhiwei Liu, Maria Cavallo, Amber Y. Gunderwala, Matthew Connolly, and Zhihong Wang[1]

From the Department of Chemistry & Biochemistry, University of the Sciences, Philadelphia, Pennsylvania 19104

Edited by Alex Toker

Class 3 mutations in *B-Raf* proto-oncogene, Ser/Thr kinase (BRAF), that result in kinase-impaired or kinase-dead BRAF have the highest mutation frequency in *BRAF* gene in lung adenocarcinoma. Several studies have reported that kinase-dead BRAF variants amplify mitogen-activated protein kinase (MAPK) signaling by dimerizing with and activating WT *C-Raf* proto-oncogene, Ser/Thr kinase (CRAF). However, the structural and functional principles underlying their activation remain elusive. Herein, using cell biology and various biochemical approaches, we established that variant BRAF^{D594G}, a kinase-dead representative of class 3 mutation-derived BRAF variants, has a higher dimerization potential as compared with WT BRAF. Molecular dynamics simulations uncovered that the D594G substitution orients the αC-helix toward the IN position and extends the activation loop within the kinase domain, shifting the equilibrium toward the active, dimeric conformation, thus priming BRAF^{D594G} as an effective allosteric activator of CRAF. We found that B/CRAF heterodimers are the most thermodynamically stable RAF dimers, suggesting that RAF heterodimers, and not homodimers, are the major players in determining the amplitude of MAPK signaling in cells. Additionally, we show that BRAF^{D594G}:CRAF heterodimers bypass autoinhibitory P-loop phosphorylation, which might contribute to longer duration of MAPK pathway signaling in cancer cells. Last, we propose that the dimer interface of the BRAF^{D594G}:CRAF heterodimer may represent a promising target in the design of novel anticancer therapeutics.

The mitogen-activated protein kinase (MAPK)[2] pathway is important in regulating cell proliferation and survival. The duration and amplitude of MAPK signaling are mainly controlled by the RAF Ser/Thr kinase family (ARAF, BRAF, and CRAF), that contain three conserved regions (CR) for membrane recruitment (CR1), N-terminal 14-3-3 regulation (CR2), and catalysis (CR3) (1). Among the three RAF isoforms, BRAF has the highest basal activity and is most frequently mutated in 7–8% of all human cancers (2). The high mutation propensity in cancer led to extensive interest in the development of BRAF-specific drugs.

WT BRAF requires RAS-initiated membrane recruitment and homo- or heterodimerization with other RAF isoforms for activation. Although all BRAF mutations trigger constitutive activation of MAPK signaling in cancer cells, they have distinct activation mechanisms and have been grouped into three main classes to reflect different biochemical properties: RAS- and dimer-independent (class 1), RAS-independent but dimer-dependent (class 2), and RAS- and dimer-dependent (class 3) (3). Class 1 mutations include the most common BRAF mutation, V600E, which accounts for ~90% of all BRAF mutations (2). The prominence of BRAF^{V600E} led to Food and Drug Administration (FDA) approval of two ATP-competitive drugs, vemurafenib and dabrafenib (4). These ATP-competitive drugs elicit effective clinical outcomes for melanoma patients carrying the V600E mutation; however, paradoxical activation and drug resistance restrict their application to cancers driven by class 2 and 3 BRAF mutations (3, 5, 6).

Inactivating BRAF mutations, class 3, are currently the most common BRAF mutation in lung adenocarcinoma (7). Herein, we study a representative of class 3 BRAF mutations, BRAF^{D594G}, which is the most frequent kinase-dead mutation. Asp-594 is part of the highly conserved DFG motif found in all kinases. The aliphatic residues Phe/Gly help to maintain the closed inactive conformation by occupying the ATP binding pocket, whereas the Asp residue is a key catalytic residue involved in Mg^{2+} coordination for the phospho-transfer reaction. Therefore, the mutation of Asp-594 to Gly prevents Mg^{2+} coordination, rendering BRAF catalytically inactive.

Intriguingly, the "kinase-dead" BRAF mutation has been validated as a driver of lung carcinoma (8, 9), suggesting that BRAF has functions that are not limited to catalyzing MEK phosphorylation but extend to other roles that are independent of enzyme activity. In parallel, the FDA-approved BRAF inhibitors inhibit the catalytic activity of WT BRAF while boosting the

This work was supported by the W. W. Smith Charitable Fund and NIGMS, National Institutes of Health, Grant 1R15GM128099-01 (to Z. W.) and the Spiers Fellowship (to N. J. C. and A. Y. G.). The authors declare that they have no conflicts of interest with the contents of this article. The content is solely the responsibility of the authors and does not necessarily represent the official views of the National Institutes of Health.

This article contains Figs. S1–S4.

[1] To whom correspondence should be addressed. Tel.: 215-596-7082; E-mail: z.wang@usciences.edu.

[2] The abbreviations used are: MAPK, mitogen-activated protein kinase; CR, conserved region(s); FDA, Food and Drug Administration; MEK, mitogen-activated protein kinase kinase; CD, catalytic domain; AUC, analytical ultracentrifugation; MD, molecular dynamics; PDB, Protein Data Bank; aa, amino acid(s); H-bond, hydrogen bond; AMPK, 5′ AMP-activated protein kinase; EGFR, epidermal growth factor receptor; SB, SB-590885; PB, PB-PLX7904; AZ, AZ-628; DSF, differential scanning fluorimetry; ATPγS, adenosine 5′-*O*-(thiotriphosphate); DMEM, Dulbecco's modified Eagle's medium; PEI-MAX, polyethyleneimine hydrochloride-MAX; ERK, extracellular signal-regulated kinase; MBP, maltose-binding protein.

noncatalytic function of BRAF to further up-regulate the MAPK signaling, which leads to secondary malignancies in clinic (5, 6, 10). This phenomenon, known as "paradoxical activation," is a major concern surrounding current BRAF inhibitors. Apparently, ATP-competitive inhibitors rearrange the structural elements of BRAF kinase to augment the noncatalytic functions, resulting in fundamentally different biological outcomes. Our current view of RAF regulation is mainly derived from mechanistic studies of enzymatically active RAF kinases by evaluating their catalytic capability. The biochemistry of noncatalytic BRAF functions is poorly understood.

The unknown noncatalytic behavior of BRAF generates therapeutic limitations of ATP-competitive RAF drugs, including paradoxical activation and drug resistance. It remains a challenge to directly target kinase-dead BRAF mutants with traditional ATP-competitive inhibitors. Novel approaches are urgently needed. Here, we integrate biophysical, biochemical, and computational approaches together with cellular assays to explore the noncatalytic function of BRAF in cancer. Additionally, our study sheds light on the activation and regulation mechanism of RAF kinase family under physiological and pharmacological conditions.

Results

BRAF^{D594G} is more prone to dimerization than WT BRAF

Dimerization through the kinase domain is required for WT BRAF and non-Val-600 BRAF mutations to function in normal and cancerous cells (8, 11). Previously, Heidorn *et al.* (12) have shown that kinase-dead BRAF^{D594A} dimerizes with CRAF when transiently transfected into D04 NRAS^{Q61L} cancer cells, and Yao *et al.* (8) determined that BRAF^{D594G} has a stronger binding potential than WT BRAF to RAS. To complement the previous cellular studies, we examined how this mutation affects the biochemical properties of BRAF in its purified form. Thus, we purified the catalytic domain (CD) of BRAF^{D594G} from *Escherichia coli* through affinity and size-exclusion chromatography with a purity of >90% suitable for biophysical analyses (Fig. 1*A*). CD-BRAF^{D594G} was subjected to velocity analytical ultracentrifugation (AUC) to determine the mass of macromolecules in solution. The majority of our protein sedimented with a sedimentation coefficient (*s*) of ~3.8 S, which relates to dimeric BRAF identified previously by Grasso *et al.* (13) (Fig. 1*B*). WT CD-BRAF and a small population of CD-BRAF^{D594G} exist at ~2.6 *s*, which relates to monomeric BRAF, previously identified by our laboratory and others (Fig. 1*B*) (13–15).

Next, we conducted molecular dynamics (MD) simulations on monomeric and dimeric WT BRAF and monomeric BRAF^{D594G} to elucidate the structural basis for enhanced dimerization. The starting structures are WT monomeric (PDB entry 4WO5 (14)) and dimeric (PDB entry 4E26 (16)) kinase domain, respectively. The BRAF^{D594G} initial structure is constructed by mutating the WT monomer crystal structure (PDB entry 4WO5 (14). The inhibitors in the crystal structure were removed. We did not include ATP molecules, because BRAF^{D594G} mutation disables ATP binding (Fig. S1). One hallmark of BRAF activation is the movement of the αC-helix, with respect to orientation toward the C-lobe, from OUT (inactive) to IN (active) conformation. The production runs of the simulations were carried out for 200 – 400 ns. The distances between the center of masses of the αC-helix and the C-lobe were measured as on average 30 ± 0.44, 28.5 ± 0.45, and 25.6 ± 0.30 Å, for monomeric BRAF^{WT}, monomeric BRAF^{D594G}, and dimeric BRAF^{WT}, respectively. This emphasizes that the αC-helix of monomeric BRAF^{D594G} is closer to the C-lobe than the monomeric WT counterpart (Fig. 1, *C* and *D*). In the αC-helix-IN conformation, residues in the αC-helix stabilize RAF dimers through hydrophobic interactions (Arg-509 with Trp-450) and H-bonds (Arg-509 with Thr-508/Arg-506/Leu-505). Our previous MD simulations together with structures of monomeric BRAF kinase domain support that a fully extended activation loop stabilizes active BRAF, whereas a rigid secondary-structure element, termed helix AS-H1, maintains an inactive conformation of BRAF (14, 17). The possibility of forming secondary structures, including 3_{10} helix and α-helix, were summarized in Table 1. The MD simulations show that the activation loop of BRAF^{D594G} is in a transition between the AS-H1 and extended loop, which is supported by the loss of the α-helical structure of the activation loop, whereas aa 598 – 600 form a short 3_{10} helix (Fig. 1 (*D* and *E*) and Table 1). The formation of the 3_{10} helix is a product of the torsional strain placed on the N terminus of the activation loop as the C terminus unwinds.

Together, these observations support that monomeric CD-BRAF^{D594G} adopts a partially active conformation indicating higher dimerization potential than CD-BRAF^{WT}, as demonstrated by the AUC data (Fig. 1*D*). Additionally, adopting the partially activated state instead of fully activated state minimizes BRAF^{D594G} homodimerization that occurs when the αC-helix and activation loop are fully IN and extended, as evidenced by oncogenic BRAF^{V600E} (17).

Dimerization potential correlates with the kinase activity of RAF dimers

It was previously established that BRAF:CRAF heterodimers are the most active RAF dimers *in vitro* (15). It remains elusive how this translates to ERK hyperactivation by BRAF^{D594G}:CRAF. In light of this, we transfected CRAF alone or co-transfected BRAF:CRAF or BRAF^{D594G}:CRAF into HEK293T cells and immunoprecipitated MBP-tagged CRAF using amylose resin to obtain either CRAF alone or BRAF:CRAF and BRAF^{D594G}:CRAF heterodimers, respectively. We added the MBP tag to enhance the solubility of CRAF for our *in vitro* experiments. The heterodimers have much higher activity than CRAF in cells and *in vitro* (Fig. 2, *A* and *B*). The activity of BRAF^{D594G}:CRAF is comparable with that of BRAF:CRAF. Thus, the kinase activity of BRAF is dispensable for transactivation of CRAF. Additionally, the observed high kinase activity rules out the possibility of forming stable RAF homodimers, as both BRAF^{D594G} and CRAF homodimers have no or very minimal kinase activity. This is consistent with our previous studies on BRAF:CRAF heterodimers, which demonstrated that separately purified BRAF and CRAF homodimers form stable BRAF:CRAF heterodimers after mixing *in vitro* (15).

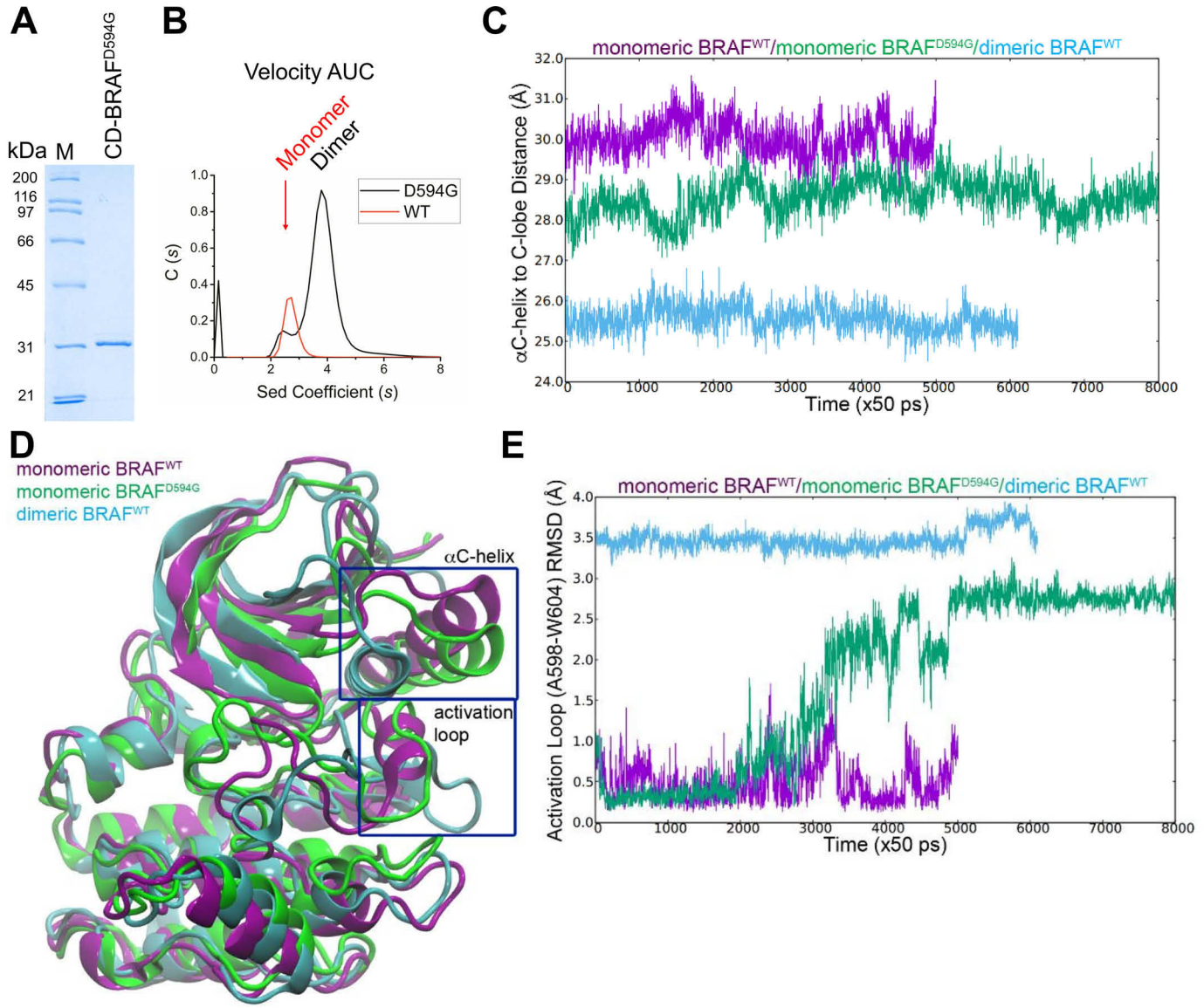

Figure 1. Catalytic domain of BRAF^{D594G} has increased dimerization in solution as compared with its WT counterpart. *A*, CD-BRAF^{D594G} was purified and analyzed by Coomassie Blue–stained SDS-PAGE. The molecular weight marker (*M*) and CD-BRAF^{D594G} are identified *above* the gel. *B*, purified CD-BRAF^{D594G} and WT CD-BRAF were investigated using velocity AUC. Monomeric BRAF or dimeric BRAF is *labeled above* the *image* at ~2.5 or ~4 *s*, respectively. *C*, molecular dynamics trajectory signifying the center of mass distance from the αC-helix toward the C-lobe as a function of simulation time are shown for monomeric WT CD-BRAF (*violet*), monomeric CD-BRAF^{D594G} (*green*), and dimeric WT CD-BRAF (*blue*). *D*, overlay of the representative snapshot from the MD simulations for monomeric WT CD-BRAF (*violet*), CD-BRAF^{D594G} (*green*), and dimeric WT CD-BRAF (*blue*). The αC-helix and activation loop are *highlighted* with *dark blue boxes*. *E*, the stability of the activation loop for monomeric WT CD-BRAF, CD-BRAF^{D594G}, and dimeric WT CD-BRAF was measured by looking at the root mean square deviation (*RMSD*), with respect to the average structure of monomeric WT CD-BRAF (featuring the AS-H1 helix throughout the whole trajectory).

Table 1
Secondary structure analysis of the activation loop

	BRAF^{WT} monomer		BRAF^{D594G} monomer[a]		BRAF^{WT} dimer[b]	
Residue	3_{10} helix	α helix	3_{10} helix	α helix	3_{10} helix	α helix
Ala-598	0.000	0.975	0.637	0.000	0.000	0.000
Thr-599	0.000	0.975	0.637	0.000	0.000	0.000
Val-600	0.006	0.986	0.637	0.000	0.000	0.000
Lys-601	0.008	0.986	0.009	0.000	0.000	0.000
Ser-602	0.142	0.584	0.008	0.000	0.000	0.000
Arg-603	0.142	0.445	0.008	0.000	0.008	0.000
Trp-604	0.138	0.011	0.008	0.000	0.010	0.000

[a] Analysis done on trajectory >240 ns (*i.e.* >4800 time (×50 ps) in Fig. 1*E* above).
[b] Result of protomer A is shown; result of protomer B is almost identical to A.

As mentioned previously, D594G is commonly found in lung cancer. To observe what effects lung cancer cells have on heterodimer activity, we performed a similar experiment in HTB-177 (KRAS^{Q61H}) lung cancer cells. For this experiment, we transfected CRAF, D594G:CRAF, and BRAF:CRAF in HTB-177 cells and monitored their activity (Fig. S2). As expected,

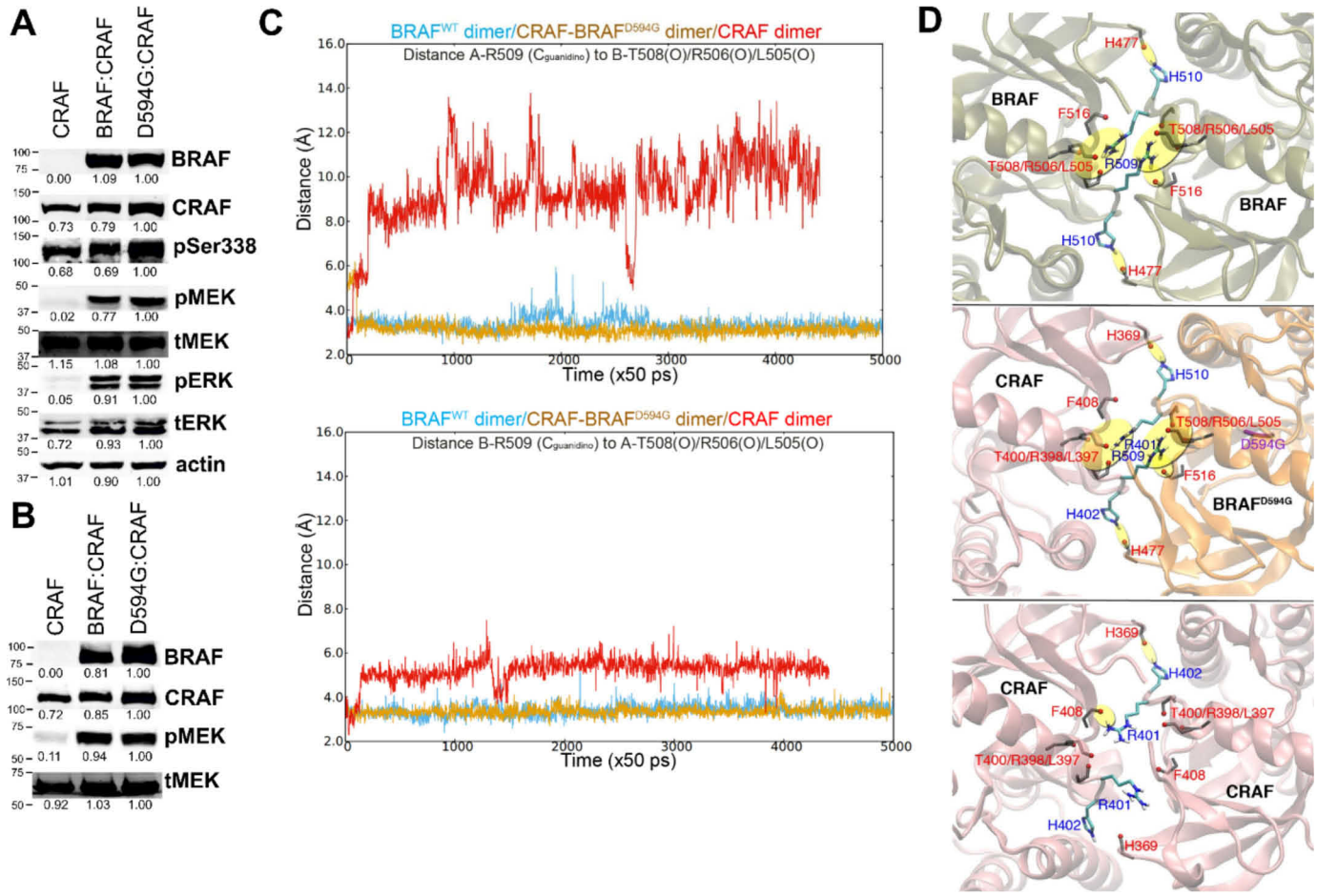

Figure 2. Heterodimers have stronger dimer interfaces than homodimers. *A*, CRAF, BRAF:CRAF, and D594G:CRAF were transiently transfected into HEK293 cells, and the lysates were probed for the indicated proteins using immunoblotting. *B*, CRAF, BRAF:CRAF, and D594G:CRAF co-immunoprecipitated from cell lysates were incubated with purified MEK1^{K97M} to measure their respective activities by probing for phospho-MEK (*pMEK*). The Western blots are representative of three independent replicates. The relative intensity values were calculated in ImageJ and are shown *below* the blot. The molecular mass values (kDa) *above* and *below* the band are indicated to the *left* of the blot. *C*, molecular dynamics trajectory measuring the distance between the conserved Arg residue's guanidino C (*BRAF:R509/CRAF:R401*) and the center of an H-bonding acceptor pocket on the other protomer across the dimer interface BRAF:BRAF (*blue*), CRAF:D594G (*gold*), and CRAF:CRAF (*red*). H-bonding from protomer A to protomer B is shown at the *top*, whereas protomer B to A is shown *below*. *D*, representative snapshots of the dimer interfaces of BRAF:BRAF (*gray*:*gray*, *top*), CRAF:D594G (*pink*:*gold*, *middle*), and *CRAF*:*CRAF* (*pink*:*pink*, *bottom*). The key hydrogen bond contacts are emphasized with *yellow highlights*.

BRAF^{D594G}:CRAF heterodimer activity is similar to that of BRAF:CRAF. This confirms that activity of BRAF is expendable for activation of CRAF. Additionally, the elevated activity in the presence of heterodimers establishes the necessary signaling output for transformation in cancer cells.

To understand why the BRAF:CRAF heterodimer forms readily, we applied MD simulations to investigate the atomistic details of BRAF:CRAF heterodimerization. We started with the dimeric CRAF (PDB entry 3OMV (6)) and dimeric BRAF (PDB entry 4E26 (16)) crystal structures with any bound inhibitors removed. The BRAF^{D594G}:CRAF heterodimer is constructed by replacing one protomer of the BRAF dimer with a CRAF protomer (extracted from the CRAF dimer structure) via alignment between the incoming and outgoing protomer, as well as introduction of D594G mutation to the remaining BRAF protomer. The production simulations of BRAF:BRAF, BRAF^{D594G}:CRAF, and CRAF:CRAF were carried out for 200–300 ns. By comparing the gain or loss and the strength of H-bonds, we conclude that BRAF:CRAF heterodimers are thermodynamically more stable than the corresponding homodimers. The interprotomer interaction can be illustrated by analyzing the distance between BRAF:CRAF Arg-509/Arg-401 (H-bond donors) and their corresponding H-bonding partners on the other protomer (Fig. 2, *C* and *D*). The calculated distance (~3 Å) for BRAF:CRAF and BRAF:CRAF dimers is ideal for H-bond formation between two protomers, but not for CRAF:CRAF dimer. In addition to the Arg-509 H-bonds, BRAF^{D594G}:CRAF heterodimers have strong interprotomer interactions between the following donor/acceptor pairs: His-510/His-369, His-402/His-477, and Arg-398/Asp-448. The average number of H-bonds (Table 2) is the sum of the fraction of H-bonds that occur in the simulations during a period of 150–200 ns. Thus, the BRAF^{D594G}:CRAF heterodimer forms the strongest dimer, followed by BRAF:BRAF, and the CRAF:CRAF homodimer is the weakest of the three.

Together, the increased dimerization potential of the heterodimer is reflected by the increased BRAF:CRAF heterodimer activity *in cellulo* and *in vitro*. CRAF homodimer forms the weakest dimer, reinforcing the notion that CRAF has the lowest basal activity alone.

Table 2
Strength of key hydrogen bond interactions

H-bond donor[a]	H-bond acceptor[a]	WT BRAF dimer	CRAF-BRAF^{D594G}	CRAF dimer
A-Arg-509[b]	B-Thr-508/Arg-506/Leu-505	1.51	1.60	0.00
B-Arg-509	A-Thr-508/Arg-506/Leu-505	1.69	1.66	0.00
A-Arg-509	B-Phe-516	0.69	0.98	0.00
B-Arg-509	A-Phe-516	0.12	0.00	0.99
A-His-510	B-His-477	0.84	0.84	0.32
B-His-510	A-His-477	0.97	0.95	0.00
A-Arg-506	B-Asp-448	0.00	2.00	0.00
B-Arg-506	A-Asp-448	1.33	0.00	0.00
Average number of H-bonds		7.15	8.03	1.31

[a] H-bond donors are guanidino NH in Arg or NH in His; H-bond acceptors are carbonyl oxygens or carboxylate oxygens in Asp-448.
[b] BRAF(CRAF) residue ID equivalency: Arg-509(Arg-401), Thr-508/Arg-506/Leu-505(Thr-400/Arg-398/Leu-397), His-510(His-402), His-477(His-369), Asp-448(Tyr-340).

The stability of BRAF^{D594G}:CRAF heterodimers is 14-3-3–dependent

The formation of BRAF:CRAF heterodimers occurs in normal cells through RAS-induced membrane recruitment (5, 6, 18, 19). The factors promoting dimerization of oncogenic BRAF^{D594G}:CRAF remain controversial. In light of this, we created a series of BRAF^{D594G} truncation constructs: ΔN-tail (region containing the BRAF-specific region), ΔRAS-binding domain (ΔRBD), ΔCR2, and ΔSSDD by truncating from the N-terminal toward the kinase domain to identify which regions of BRAF^{D594G} are crucial for dimerization with CRAF (Fig. 3*A*). We transiently transfected the BRAF^{D594G} deletion constructs: ΔN-tail, ΔRAS-binding domain (ΔRBD), ΔCR2, and ΔSSDD into HEK293 cells with or without WT CRAF (Fig. 3*B*). The BRAF^{D594G} constructs and CRAF have poor expression as single transfections, but when co-transfected together, the expression increases on average 9- and 2-fold for BRAF^{D594G} and CRAF, respectively, suggesting that formation of BRAF^{D594G}:CRAF protects both proteins from degradation. The observed change in expression of both BRAF and CRAF can be used as a tool to determine whether heterodimer pairs form in cells. All of the BRAF^{D594G} constructs containing the SSDD motif were able to stabilize CRAF (Fig. 3*B*). It is not surprising that ΔSSDD lost the ability to activate CRAF, as the SSDD motif is important for proper regulatory spine alignment, which is a prerequisite for dimerization and activation of RAF family members (13).

14-3-3 chaperone protein binding to pSer-729 of BRAF enhances homo- or heterodimerization of WT RAF (20, 21). AMPK has been identified to phosphorylate the BRAF C-terminal 14-3-3–binding site, Ser-729 (21). To verify the effect of 14-3-3 on BRAF^{D594G}:CRAF dimerization, we treated cells expressing RAF heterodimers with dorsomorphin 2HCl (compound C), a potent AMPK inhibitor. The phosphorylation of Raptor, a well-established protein substrate of AMPK, was decreased in the presence of compound C, verifying that AMPK is potently inhibited (Fig. 3*C*). Additionally, total CRAF, pCRAF, and pSer-729 were decreased in the context of the BRAF^{D594G}:CRAF heterodimer (Fig. 3*C*). To further verify the role of 14-3-3 binding, we introduced the S729A mutation to mimic unphosphorylated BRAF^{D594G}. Unfortunately, BRAF$^{D594G/S729A}$ was not expressed well in HEK293 cells, preventing more detailed investigation. This is consistent with the findings of Park *et al.* (22), who show that the mutation to S729A results in poor stability of purified BRAF from insect or mammalian cells. Regardless, the observed destabilization by the S729A mutation together with the compound C data suggest that 14-3-3 binding to pSer-729 stimulates BRAF^{D594G}:CRAF heterodimerization and subsequent CRAF activation. Because phosphorylation of Ser-729 was not completely depleted by the AMPK inhibitor, these results suggest that there are other kinases, other than AMPK, that are responsible for Ser-729 phosphorylation. In parallel, AMPK inhibitor has little effect on pSer-729 and pCRAF-Ser-338 in the context of WT BRAF:CRAF heterodimers, suggesting that they have a distinct regulation mechanism.

BRAF^{D594G}:CRAF heterodimers bypass autoinhibitory phosphorylation in cancer cells

We previously identified that BRAF^{WT} can autophosphorylate its P-loop (Ser-465/Ser-467) to inactivate itself in the absence of native substrate MEK (15). By doing so, BRAF is subject to fine-tuned regulation to ensure rapid termination of RAF signaling. To determine whether BRAF:CRAF and BRAF^{D594G}:CRAF use a similar mechanism, we incubated these kinases with ATP for 30 min to let autophosphorylation complete prior to quantifying their specific activity. The activity of BRAF:CRAF was decreased by ~40–50% upon autophosphorylation (Fig. 4*A*), suggesting that autophosphorylation of certain residues negatively regulates the kinase activity of BRAF. Intriguingly, no obvious change was detected for BRAF^{D594G}:CRAF (Fig. 4*A*), demonstrating that oncogenic mutations can bypass autophosphorylation to sustain pathway signaling. To further verify this finding, we monitored total BRAF autophosphorylation via ^{32}P autoradiograph. As shown in Fig. 4*B*, BRAF^{WT} was able to autophosphorylate itself and MEK; however, BRAF^{D594G}:CRAF could only phosphorylate BRAF^{D594G} and MEK, and not CRAF (Fig. 4*B*). The lack of CRAF phosphorylation within BRAF^{D594G}:CRAF dimers provides compelling evidence that RAF autophosphorylation occurs in *trans*, not in *cis*.

To further verify this model, we introduced the R509H mutation, a mutation known to disrupt the "side-to-side" dimer interface of BRAF, to BRAF^{V600E}. As monomeric BRAF$^{V600E/R509H}$ is still active, our data clearly demonstrate that autophosphorylation requires an intact dimer interface and occurs as *trans*- rather than *cis*-autophosphorylation (Fig. 4, *A* and *B*). Our finding highlights the physiological significance of the "side-to-side" dimer interface, other than allosteric *trans*-activation. Within a BRAF dimer, BRAF *trans*-phosphorylates both activation loop and inhibitory phosphorylation sites to fine-tune the overall BRAF activity (Fig. 4, *A* and *B*) (15, 17).

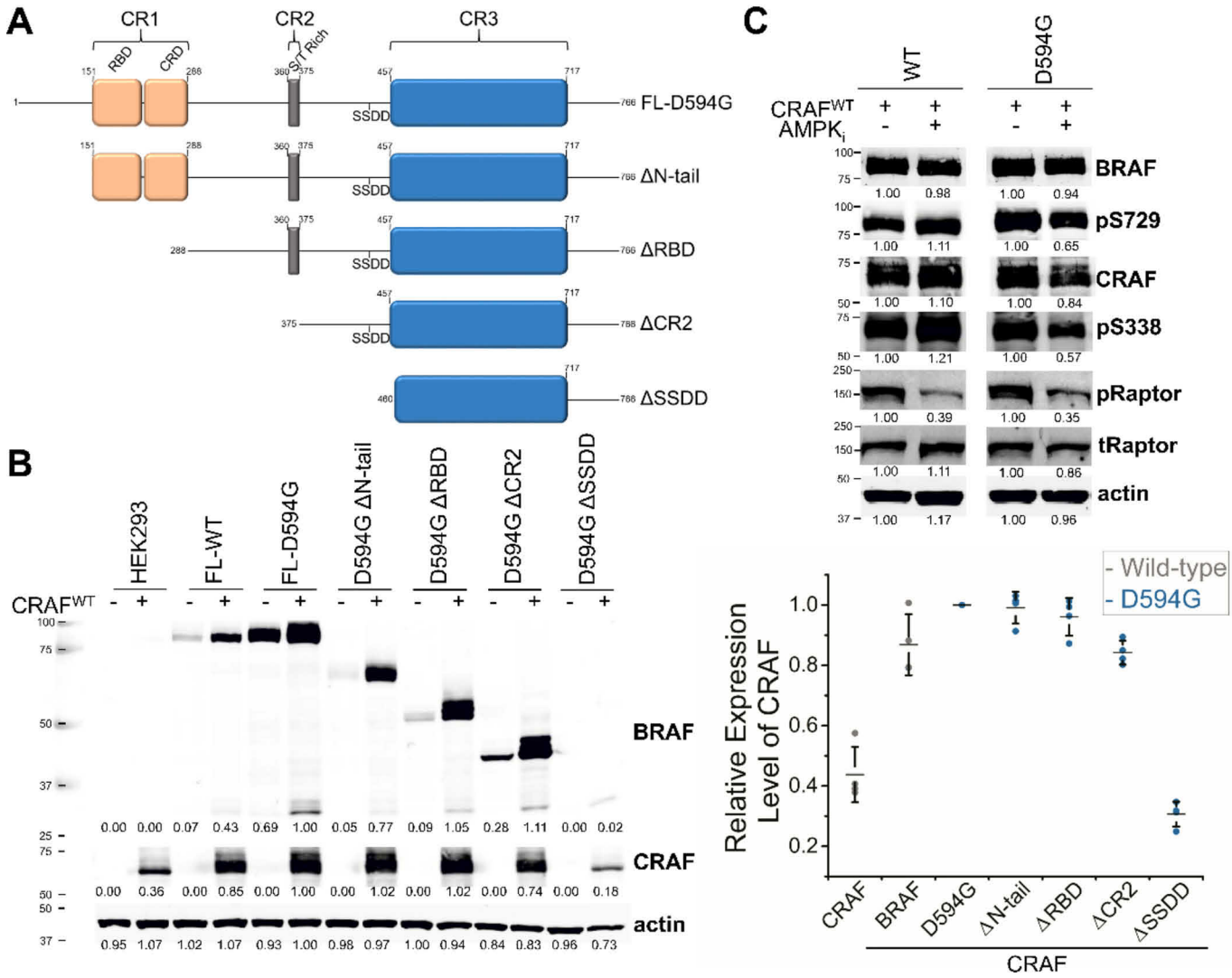

Figure 3. The stability of BRAF^{D594G} and CRAF is dependent on heterodimerization. *A*, *schematic diagram* of the deletion mutants of BRAF^{D594G}. In FL-D594G, the conserved regions (CR1–3) and specific motifs are *labeled*. The amino acid numbers are identified for the beginning/end of the construct and conserved regions. The RAS-binding domain (*RBD*), cysteine-rich domain (*CRD*), serine/threonine-rich domain (*S/T Rich*), SSDD (aa 446–449), and kinase domain are *labeled* accordingly. *B*, the indicated constructs were transiently transfected into HEK293 cells. We examined the expression changes of D594G in the presence and absence of CRAF in cells cultured under 10% fetal bovine serum. A scatter plot is shown with the individual points and the average ± S.D. (*error bars*). The relative expression level of CRAF indicates CRAF expression alone or in the presence of WT BRAF or D594G constructs that are all normalized to FL-BRAF^{D594G}. *C*, 5 μM compound C, an AMPK inhibitor (*AMPK$_i$*), was added to HEK293 cells expressing either BRAF:CRAF or D594G:CRAF for 4 h. ImageJ was used to calculate the relative intensity values, which are shown *below* the blot. The molecular mass values (kDa) are shown to the *left* of the blot.

P-loop phosphorylation destabilizes BRAF dimers

Our mechanistic studies identified that P-loop phosphorylation negatively regulates the kinase activity of BRAF^{WT} (17). We carried out MD simulations on dimeric BRAF^{WT} kinase domain with P-loop phosphorylation (pSer-465/pSer-467) and compared it with the simulations of WT unphosphorylated dimer. Both simulations started from the same crystal structure (PDB entry 4E26 (16)). Our MD data demonstrate that phosphorylation of the P-loop disfavors dimer formation by disrupting multiple H-bonds in the dimer interface, whereas these H-bonds remained intact in the unphosphorylated dimer (Fig. 4*C*). In addition, the two phosphorylated protomers also moved apart from each other (*black trajectory*, Fig. 4*C*), relative to the unphosphorylated protomers (*blue trajectory*, Fig. 4*C*), further validating the distorted dimer configuration. Other dimer simulations, including WT dimer and P-loop phosphorylation with inhibitors and WT dimer with the R509H mutation, show consistent results of weakened dimeric interaction upon P-loop phosphorylation or introduction of the R509H mutation (Fig. S3). Consistent with our MD simulations, co-immunoprecipitation experiments verified that introduction of the phosphomimetic mutation S465D/S467D (SS/DD) to the P-loop compromised the dimerization ability of BRAF, as shown in Fig. 4*D*. Together, we conclude that P-loop phosphorylation decreases the formation of BRAF dimers and most likely displaces the αC-helix to an OUT position that leads to an inactive conformation.

Inhibiting the catalytic activity of CRAF within the BRAF^{D594G}:CRAF

The two FDA-approved BRAF drugs dabrafenib and vemurafenib have a positive clinical outcome for patients harboring oncogenic BRAF^{V600E}, but are less effective toward non-Val-

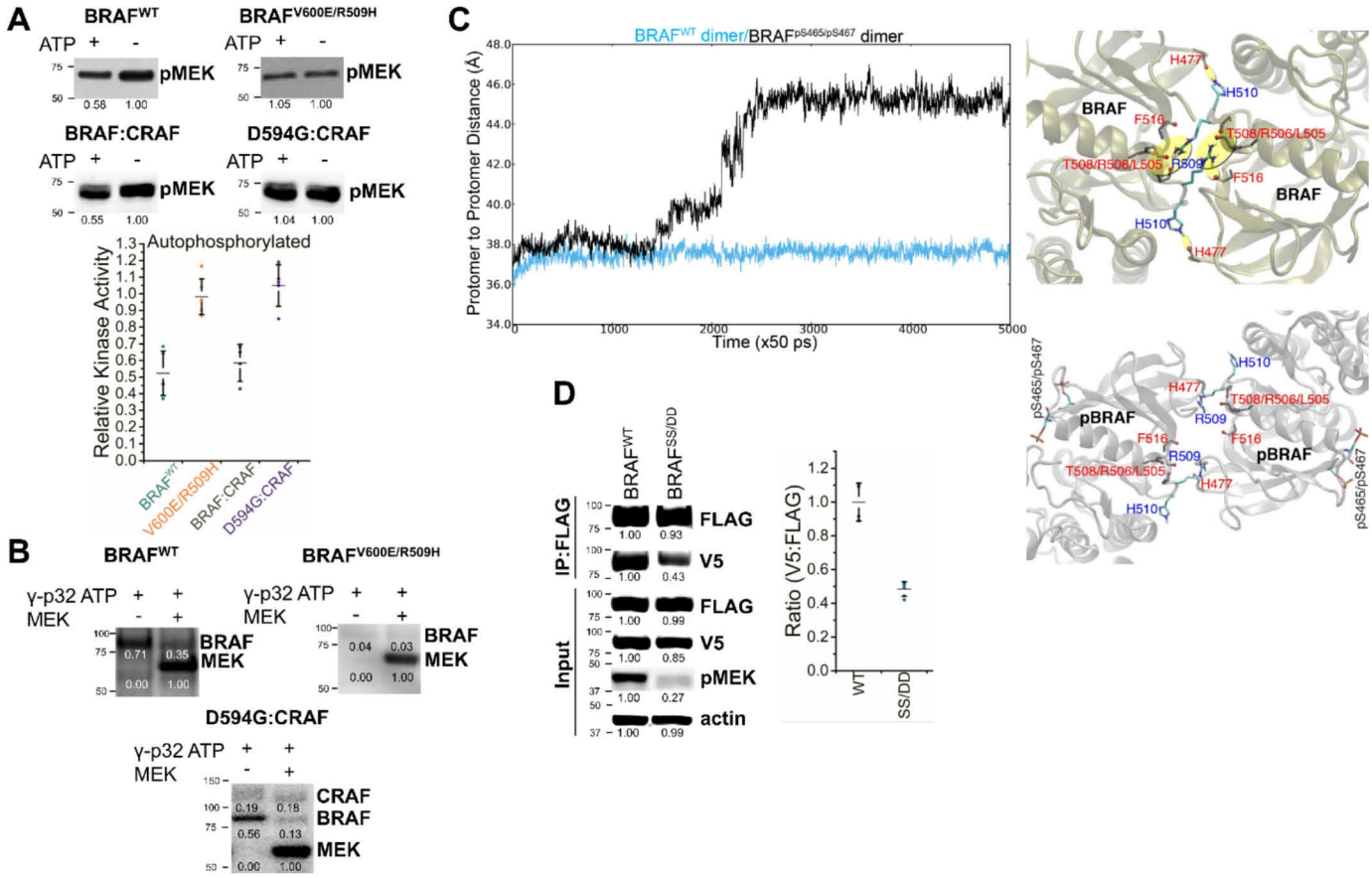

Figure 4. Inhibitory autophosphorylation of the P-loop disrupts dimerization of WT BRAF and is bypassed by BRAF^{D594G}:CRAF heterodimers. *A*, WT BRAF, BRAF$^{V600E/R509H}$, BRAF:CRAF, and D594G:CRAF were preincubated with ATP (+) or without ATP (−) for 30 min at room temperature to allow the completion of autophosphorylation and then were incubated with MEK1^{K97M} for 10 min at 30 °C. The relative kinase activities of unphosphorylated RAF protein (*Native*) and autophosphorylated RAF protein (*Auto*) were quantified to the respective native lanes of three independent experiments ± S.D. (*error bars*) and are shown *below* the immunoblots. A scatter plot is shown of the relative kinase activity of the autophosphorylated lanes normalized to the respective native lane. *B*, ^{32}P-labeled ATP was incubated with WT BRAF, BRAF$^{V600E/R509H}$, and D594G:CRAF in the presence and absence of MEK1^{K97M} for 30 min before being subjected to SDS-PAGE radiograph gel imaging. Autophosphorylation of RAF and phosphorylation of MEK1^{K97M} were recorded simultaneously. *C*, molecular dynamics simulations monitoring the protomer distance of WT BRAF or P-loop phosphorylated BRAF (pSer-465/pSer-467) were examined. The trajectory of the dimer interface was tracked for WT BRAF (*blue*) and pSer-465/pSer-467-BRAF (*black*). Snapshots showing the dimer interface for WT BRAF (*top*) and pSer-465/pSer-467-BRAF (*bottom*) are shown to the *right*. Hydrogen-bonding interactions are indicated by *yellow circles*. *D*, WT BRAF (*BRAF^{WT}*) and BRAF S465D/S467D (*BRAF$^{SS/DD}$*) were transiently transfected into HEK293 cells. FLAG-tagged BRAF was co-immunoprecipitated from the cell lysate and then probed for V5-tagged BRAF. The ratio of V5 to FLAG is shown to the *right* of the immunoblots for three independent experiments ± S.D. The relative intensity values are *below* the blot. The molecular mass standard values (kDa) are identified to the *left* of the blot.

600 BRAF mutants (4, 9). Other laboratories have suggested that targeting MEK or EGFR is a viable treatment option for class 3 BRAF tumors (8), but currently no RAF directed therapies are available. There are three types of BRAF inhibitors, which are grouped by how they orient the αC-helix or DFG motif (4). Type I inhibitors, such as SB-590885 (SB), lock BRAF into an active conformation with αC-helix-IN and DFG-IN. Type I^{½} inhibitors, including dabrafenib, vemurafenib, PLX-4720, and PB-PLX7904 (PB), orient the αC-helix-OUT and DFG-IN conformation. Type II inhibitors, such as AZ-628 (AZ), adopt the αC-helix-IN and DFG-OUT conformation. The αC-helix-IN (type I/II) configuration allows for inhibitor binding to both protomers of BRAF with equal potency; however, type I^{½} inhibitors lock the αC-helix-OUT configuration to sterically hinder occupancy for the second protomer, which leads to negative cooperativity. Although each category of inhibitor is effective at inhibiting BRAF^{V600E} (17), they have very different binding mechanisms that regulate dimeric WT BRAF differently. WT BRAF displays drug resistance and paradoxical activation toward type I^{½} inhibitors.

Here we evaluate the different categories of RAF inhibitors against BRAF^{D594G}:CRAF heterodimers. Differential scanning fluorimetry (DSF) results show that all of the tested ATP-competitive inhibitors bind to CD-BRAF^{D594G} (Fig. 5*A*), although BRAF^{D594G} could not bind to ATP (Fig. S1). However, it remains unclear whether these inhibitors can trigger paradoxical activation in cells expressing BRAF^{D594G}. Additionally, our MD simulations have shown that the D594G:CRAF heterodimer is in a different conformation than the CRAF homodimer; therefore, different drug response is expected between RAF homo- and heterodimers. To address these concerns, we applied cell-based assays to evaluate the potency of the selected inhibitors in HEK293 cells transiently transfected with BRAF^{D594G} and CRAF. BRAF^{V600E} and WT BRAF/CRAF were used as the controls (Fig. 5, *B* and *C*).

Pan-RAF inhibitors, such as AZ, are active against ARAF, BRAF, and CRAF with equal potency; thus, titrating different

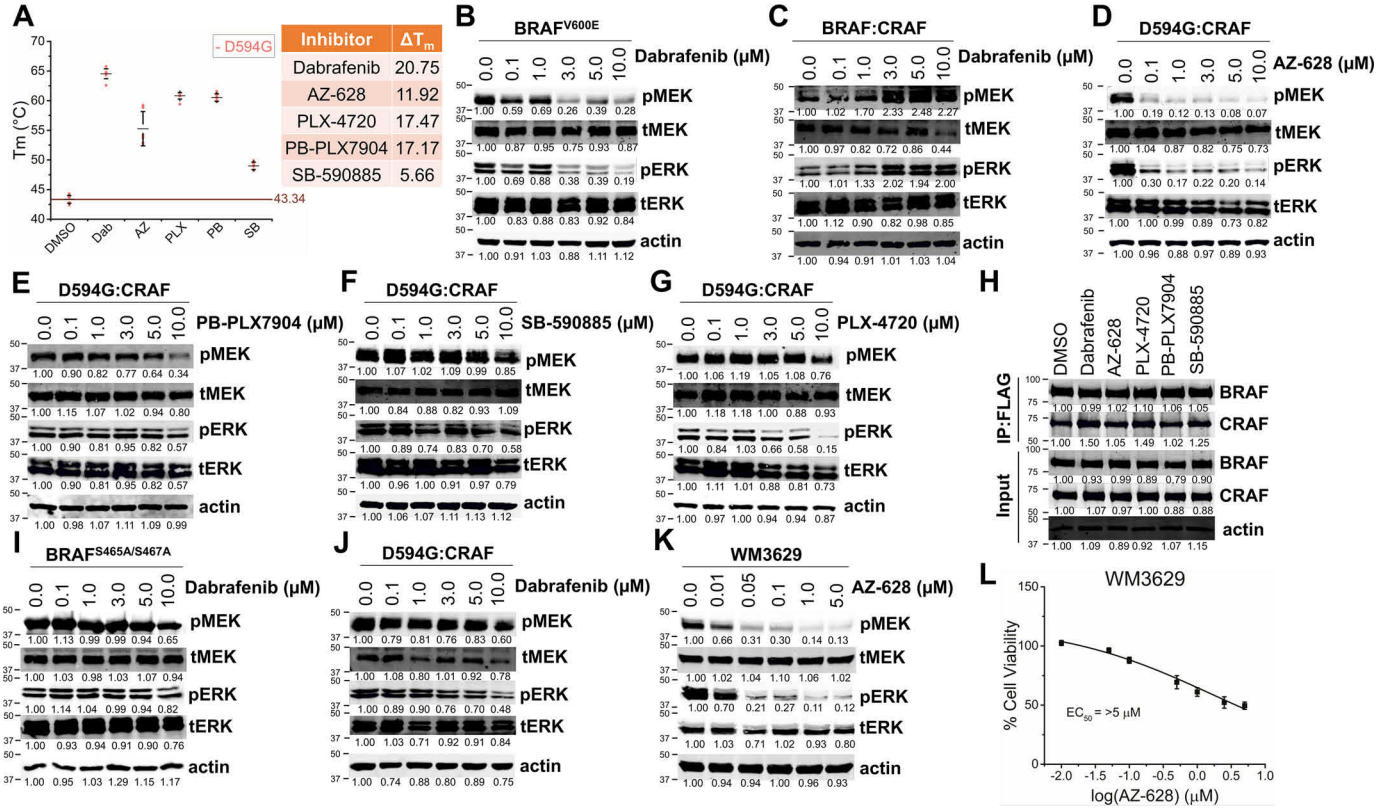

Figure 5. Targeting BRAF^{D594G}:CRAF heterodimers with ATP-competitive inhibitors displays drug resistance despite decreased MAPK signaling. *A*, 5 μM CD-D594G was incubated with 25 μM inhibitor and then subjected to DSF. The melting temperatures (T_m) of CD-D594G with DMSO, dabrafenib, AZ-628, PLX-4720, PB, and SB-590885 were plotted. The ΔT_m was calculated by subtracting CD-D594G in the presence of drug from no treatment. *B* and *G*, the respective constructs were transiently transfected into HEK293 cells and treated with inhibitor at the indicated drug concentrations for 1 h. *B* and *C*, BRAF^{V600E} and BRAF:CRAF were treated with dabrafenib. *D–G*, D594G:CRAF was treated with AZ-628 (*D*), PB (*E*), SB-590885 (*F*), and PLX-4720 (*G*). *H*, D594G:CRAF was treated with the specified drug for 1 h before lysing and then co-immunoprecipitation with anti-FLAG resin. *I* and *J*, BRAF$^{S465A/S467A}$ (*I*) and D594G:CRAF (*J*) were treated with dabrafenib in HEK293 cells. *K* and *L*, melanoma cells, WM3629, expressing BRAF^{D594G} and NRAS^{G12D} were treated with AZ-628 for 1 h for Western blot analysis (*K*) or 96 h for cell viability experiments (*L*). Cell viability was calculated by dividing the A_{450} (absorbance for the WST reagent) with AZ-628 treatment by the A_{450} for no treatment × 100. The cells were harvested and lysed with 4% SDS and then subjected to Western blotting analyses, unless otherwise indicated. The relative intensities are shown *below* the blot. The molecular mass numbers (kDa) are identified to the *left* of the blot. *Error bars*, S.D.

concentrations of AZ showed inhibition at 0.1 μM (Fig. 5*D*). The potency of AZ toward BRAF^{D594G}:CRAF is not surprising, because this inhibitor has been shown to have low nanomolar potency toward CRAF in cell-free experiments (23). Additionally, Noeparast *et al.* (24) show a similar inhibition profile toward the D594G:CRAF heterodimer. PB is a paradox-breaking inhibitor designed to minimize paradoxical activation (25), but type I½ inhibitors have much lower activity toward dimeric RAF, and no significant activity of PB toward the BRAF^{D594G}:CRAF heterodimer was observed (Fig. 5*E*). Although AZ and SB target monomeric and dimeric BRAF with similar potency, SB only shows inhibition at the highest concentration tested toward BRAF^{D594G}:CRAF (Fig. 5, *D* and *F*), most likely due to its low potency toward CRAF. We also tested PLX-4720, which is known to potently inhibit monomeric BRAF, and it only shows slight inhibition of the BRAF^{D594G}:CRAF heterodimer at the highest concentration of drug used (Fig. 5*G*). AZ, a representative of type II pan-RAF inhibitors, exhibits inhibition of the BRAF^{D594G}:CRAF heterodimer at the lowest concentrations tested. Additionally, Karoulia *et al.* (4) have identified that pan-RAF inhibitors have a slower off rate and dissociate the RAF/MEK complex. These data suggest that pan-RAF inhibitors might be a good scaffold for rationally designed BRAF^{D594G}:CRAF inhibitors.

Notably, none of the ATP-competitive inhibitors induced paradoxical activation even though binding of the DFG-IN inhibitors dabrafenib, PLX-4720, and SB shows slight enhancement of BRAF^{D594G}:CRAF heterodimerization (Fig. 5*H*). On the contrary, WT BRAF:CRAF heterodimers were paradoxically activated by dabrafenib under the same conditions (Fig. 5*C*) (24). Due to the correlation of BRAF^{D594G} and P-loop autoinhibitory phosphorylation, we introduced an S465A/S467A (SS/AA) mutation to WT BRAF to prevent P-loop phosphorylation. No paradoxical activation was observed for BRAF$^{SS/AA}$, suggesting that P-loop phosphorylation plays a role in paradoxical activation (Fig. 5*I*). Under this scenario, kinase-dead BRAF abolishes P-loop phosphorylation of catalytically active CRAF within the BRAF^{D594G}:CRAF dimer, which also evades paradoxical activation. This model is consistent with the work of Holderfield *et al.* (26), who highlighted that ATP-competitive inhibitor relieves inhibitory P-loop phosphorylation of WT RAF to trigger paradoxical activation. Another possibility is that the BRAF^{D594G} mutation already makes BRAF a perfect allosteric activator and inhibitor binding makes no further enhancement regarding its ability to transactivate CRAF (Fig. 5*J*).

We also treated melanoma cells (WM3629) that express BRAF^{D594G} and NRAS^{G12D} with AZ (Fig. 5*K*). The pan-RAF

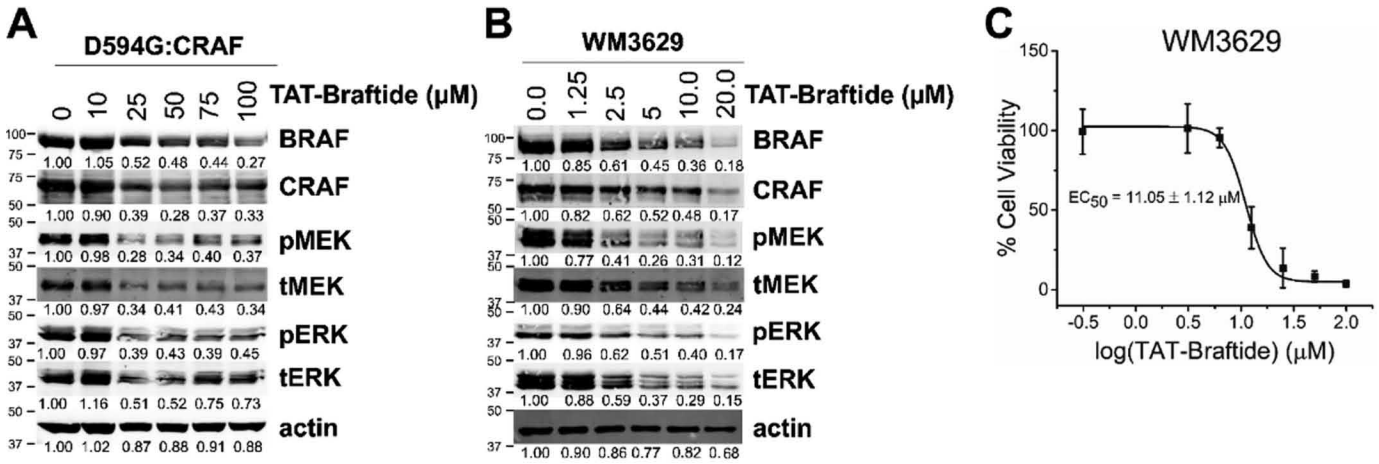

Figure 6. Targeting the dimer interface of BRAF^{D594G}:CRAF heterodimers causes both protein degradation and diminished MAPK signaling in cells. *A*, D594G:CRAF were transiently transfected and then treated with TAT-Braftide (0, 10, 25, 50, 75, and 100 μM) for 4 h. *B*, melanoma cells, WM3629, harboring BRAF^{D594G} and NRAS^{G12D} were treated with TAT-Braftide for 4 h. The cells were harvested and lysed with 4% SDS and then subjected to Western blotting analyses. *C*, WM3629 were treated with TAT-Braftide for 48 h, and then the medium was replaced with WST reagent diluted in Opti-MEM. Percentage cell viability was calculated by dividing the A_{450} with Braftide by the A_{450} for no treatment × 100. The relative intensities of the bands are located *below* the blot. The molecular mass values (kDa) are located to the *left* of the blot. *Error bars*, S.D.

inhibitor completely abolished MEK/ERK signaling at 1 μM, which indicates that AZ can inhibit the MAPK pathway in a short time period. However, long exposure of 96 h still exhibited ~50% of cell growth at the highest concentration (5 μM) of drug treated (Fig. 5*L*), suggesting that BRAF^{D594G}:CRAF heterodimers display drug resistance toward ATP-competitive inhibitors. This is consistent with another group who showed that AZ alone cannot fully eliminate growth of cells harboring various RAS mutations (27). The discrepancy between the amount of drug required for MAPK inhibition and cancer cell death highlights that pan-RAF inhibitors might not be a viable therapeutic treatment for class 3 BRAF mutations.

RAF dimer breaker is active against BRAF^{D594G}:CRAF

Recognizing that dimerization of BRAF^{D594G} and CRAF is critical for both protein stability and kinase activity poises the dimer interface as a promising drug target. Previously, we developed a 10-mer peptide (Braftide) that shows efficient inhibition and degradation of WT BRAF and BRAF^{G469A} both *in vitro* and in a variety of cells exhibiting either RAS dependence or independence, respectively (28). To extend the same study to BRAF^{D594G}:CRAF heterodimers, we titrated 0–100 μM TAT-Braftide into HEK293 cells overexpressing the BRAF^{D594G}:CRAF heterodimer (Fig. 6*A*). This peptide inhibitor shows not only inhibition of MAPK signaling, but also degradation of the BRAF^{D594G}:CRAF heterodimer at as low as 25 μM. We applied a similar experiment to WM3629 cancer cells (Fig. 6*B*). TAT-Braftide exhibits degradation of BRAF^{D594G} and CRAF at concentrations as low as 2.5 μM in WM3629 cells. We treated WM3629 cells with TAT-Braftide for 48 h to observe the activity of this peptide by cell viability assays, which showed dose-dependent inhibition of cell growth and an EC_{50} of 11.05 ± 1.12 μM (Fig. 6*C*). Together, these results highlight that BRAF^{D594G}:CRAF heterodimers are still sensitive to dimer breakers, despite the fact that it has a stronger dimer interface than BRAF homodimers.

Discussion

In our study, we focused on BRAF^{D594G}, a representative of kinase-dead BRAF mutants, to better understand the noncatalytic function of BRAF. Interestingly, protein kinases have evolved to have allosteric scaffolding properties, in addition to their inherent capability of catalyzing the transfer of the γ-phosphate from ATP to tyrosine, serine, or threonine residues in the substrate proteins. Pseudokinases are an example of enzymes that have diverged to primarily function as scaffolds, such as kinase-impaired HER3 which allosterically activate other EGFR/HER family members through asymmetric dimerization (29). Another example is kinase-suppressor of RAS (KSR) which has been shown to function as a scaffolding protein to allosterically regulate RAF and MEK (30). BRAF kinase has both scaffold function and catalytic activity that are integrated to determine the final output of RAF signaling. Intriguingly, ATP-competitive inhibitors can differentially alter the two functions to trigger paradoxical activation, in which the scaffold function of BRAF is exaggerated to compensate the inhibited kinase activity, and the overall outcome is enhanced RAF signaling. However, it is hard to pinpoint which role is more significant than the other. The kinase-dead BRAF mutant provides a valuable tool to elucidate the allosteric consequence of mutations that are linked to cancer.

Our biophysical experiments and MD simulations show that BRAF^{D594G} is more prone to dimerization than BRAF^{WT} due to the positioning of the αC-helix toward the IN conformation. In addition, the activation loop of BRAF^{D594G} is beginning to unwind from the AS-H1 loop toward full extension, which is a prerequisite for kinase activation. The extended activation loop stabilizes the regulatory spine (R-spine) and αC-helix into a conformation suitable for dimerization (30); thus, BRAF^{D594G} is in a partially active, dimerization-competent conformation leading to enhanced allosteric function. Interestingly, the most recent cryo-EM structure of BRAF in complex with ATP analog

ATPγS suggests that ATP binding is critical to maintain the autoinhibited state (22). Because BRAF^{D594G} cannot bind ATP, this feature further stabilizes the active conformation of BRAF to support RAF dimerization.

Experiments with other pseudokinases (VRK, MLKL, STRAD, ERBB3, and JAK2) have emphasized that ATP binding can enhance allosteric activation of the associated partner for some pseudokinases (31–34). However, BRAF^{D594G} does not bind ATP but still functions as an allosteric activator. In addition, the A481F or A373F mutations, which interfere with ATP binding to BRAF or CRAF, respectively, have been shown to constitutively dimerize with and activate the RAF binding partner (35). These results combined with ours suggests that the alignment of the catalytic spine is not necessary for the scaffold function of BRAF.

Enhanced signaling required to drive MAPK pathway activation in cells is attained by either increased enzyme activity or reduced negative regulatory feedback effects (36). We show that BRAF^{D594G}:CRAF heterodimers are more active than CRAF alone and have an activity that is comparable with that of the BRAF:CRAF heterodimer. This increase in activity could be attributed to BRAF^{D594G}:CRAF heterodimers bypassing inhibitory P-loop autophosphorylation that negatively controls WT RAF activity in cells (17). The glycine-rich P-loop (Gly-*X*-Gly-*X*-*X*-Gly motif) is highly conserved among protein kinases and is known to position the α-/β-phosphates of ATP for optimal γ-phosphoryl transfer during catalysis. In addition, it is believed that the hydrophobic interactions between P-loop and activation loop stabilize the inactive configuration of the kinase (37). Protein kinases share a universal activation mechanism, in which conformational changes in three conserved structural motifs at the active site (the activation loop, the DFG motif, and the αC-helix) determine the transition from the inactive to the active conformation (38). The effect of P-loop phosphorylation has not been well-studied. Our MD simulation results demonstrate that phosphorylated P-loop disfavors the side-to-side dimer configuration, which in turn supports the nonproductive position of the αC-helix. Here, we have confirmed the existence of a cross-talk among the P-loop and the three motifs that modulates the conformational equilibrium of the BRAF kinase. These data unveil P-loop as an important structural feature involved in positioning the αC-helix, depending on its phosphorylation status. Given that the Ser-465/Ser-467 residues are highly conserved among the P-loop (Fig. S4, *A* and *B*), it is appealing to propose a similar role for the conserved Ser/Thr residues in other kinase families.

Previously, the molecular mechanism of RAF regulation has been mostly derived from structures of isolated kinase domains or fragments of other domains. The cryo-EM structures of full-length BRAF-MEK1–14-3-3 complexes were solved recently (22), providing a more comprehensive structural characterization of RAF. In those structures, both autoinhibited and fully activated BRAF were captured, demonstrating that MEK1 and 14-3-3 are both involved in stabilizing BRAF in the active or inactive conformations (22). Our findings introduce an additional layer of complexity to the precise mechanism of BRAF activation. Our laboratory previously identified that the presence of MEK1 decreases overall BRAF autophosphorylation

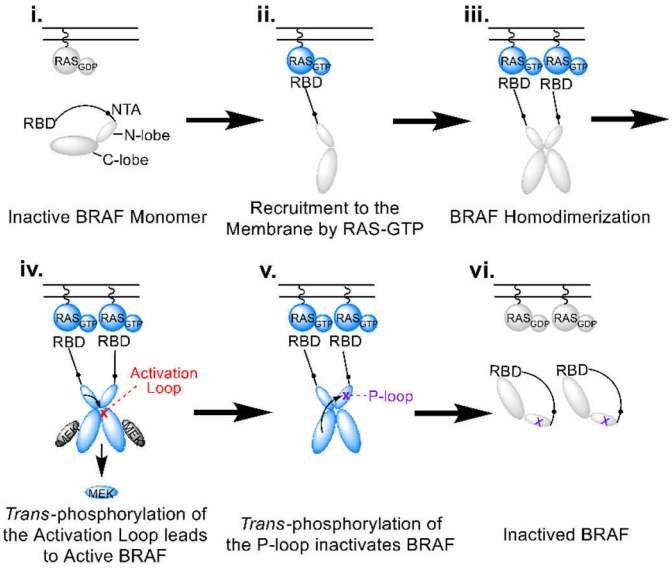

Figure 7. Stepwise activation of BRAF under physiological conditions. *i*, monomeric BRAF is found in the cytosol with the N-terminal and C-terminal interaction causing BRAF to be inactive. *ii*, active RAS stimulates the N-terminal domain of BRAF to release from the C-terminal domain. *iii*, RAS clustering brings RAF monomers in close proximity, which promotes RAF dimerization. *iv*, BRAF is stabilized by MEK that helps facilitate autophosphorylation of the activation loop (*red*). After MEK phosphorylation, BRAF and MEK dissociate, allowing active MEK to interact with ERK. *v*, BRAF regulates its activity by autophosphorylating the P-loop (Ser-465/Ser-467, *violet*), leading to inactive BRAF. *vi*, P-loop phosphorylation renders BRAF inactive, down-regulating the entire MAPK signaling cascade. The inactive kinases are shown in *gray*, whereas the active kinases are indicated by *blue*. *RBD*, RAS-binding domain; *NTA*, N-terminal acidic domain.

while increasing phosphorylation of the activation loop *in vitro*, suggesting a new allosteric role of MEK1, other than functioning as a substrate of RAF kinases (15). In light of those findings, we propose one model for RAF regulation under physiological conditions, as shown in Fig. 7. After RAS-initiated RAF dimerization, MEK binding primes the activation loop of RAF for *trans*-phosphorylation (15), which leads to maximal RAF activation and subsequent MEK phosphorylation. Upon dissociation of phosphorylated MEK, RAF *trans*-phosphorylates the P-loop to diminish its own kinase activity. Meanwhile, this negative regulation loop can be dampened by protein phosphatases to maintain the highest RAF activity. In this model, P-loop autophosphorylation is a self-sustained mechanism to self-limit its kinase activity *in vivo*.

Two main models have emerged to shed light on the molecular mechanism of paradoxical activation. The first model suggests that binding of RAF inhibitors increases dimerization of drug-bound RAF with inhibitor-free RAF, which results in RAS-dependent MEK/ERK activation (5). Similarly, Heidorn *et al.* (12) have related this model to how kinase-dead BRAF activates CRAF in a RAS-dependent manner. The second model identifies that RAF inhibitors activate MEK/ERK by relieving inhibitory RAF autophosphorylation (26). In our work, we provide evidence reconciling the two models of paradoxical activation. We show that inhibitory autophosphorylation occurs in *trans*, not in *cis*; thus, oncogenic BRAF^{D594G} can evade this negative feedback loop by eliminating autophosphorylation of CRAF in the BRAF^{D594G}:CRAF heterodimer due to the lack of enzyme activity. RAF ATP-competitive inhibitors do not dis-

play paradoxical activation in the context of BRAF^{D594G}:CRAF heterodimer, providing direct evidence that relief of P-loop phosphorylation by RAF inhibitors is capable of activating MAPK signaling. Additionally, BRAF^{D594G} and CRAF readily form a stable dimer; hence, RAF inhibitors could no longer boost the allosteric function of BRAF.

The increased frequency of non-Val-600 mutations detected in lung and other cancers highlights the urgency of targeting class 3 BRAF (39). Although there have been several proposed strategies to combat dimer-dependent BRAF mutations, such as targeting CRAF, MEK, and EGFR (3, 9, 24), there are currently no clinically approved drugs that are designed specifically to treat tumors harboring class 3 BRAF mutations. Since the approval of targeting BRAF^{V600E} mutations with vemurafenib or dabrafenib in combination with MEK inhibitors, this has been a suggested strategy to treat other BRAF mutations. Combination therapy with RAF and MEK inhibitors in cell lines harboring class 3 BRAF mutations has been analyzed previously (8, 24). These experiments show that MEK inhibitors alone or in combination with RAF inhibitors decrease MAPK pathway activation and induce cellular apoptosis. Although treatment with MEK inhibitors is promising, cytotoxicity is an inevitable concern; thus, more specific inhibitors are urgently needed. Our results on inhibiting phosphorylation of Ser-729 of BRAF make the C-terminal 14-3-3 binding site a druggable target for class 3 BRAF mutations. Similarly, Kondo *et al.* identified that targeting the αI-helix, at the 14-3-3–binding interface, could have improved therapeutic efficacy in dimer-dependent BRAF mutations (40).

Braftide activity toward BRAF^{D594G}:CRAF heterodimers in cells suggests that allosteric inhibitors targeting the dimer interface could have an improved therapeutic index. In addition, we show that pan-RAF ATP-competitive inhibitors show initial inhibition of BRAF^{D594G}:CRAF heterodimer activity, but prolonged exposure fails to abolish WM3629 cancer cell growth. Moreover, Montagut *et al.* (41) suggest that overexpression of CRAF, as we see with the co-transfection of BRAF^{D594G}:CRAF, can lead to acquired resistance to pan-RAF inhibitors, suggesting that targeting the ATP-binding pocket of CRAF alone might not be the best therapeutic strategy. Hence, rationally designed drugs with improved selectivity are required to target CRAF or the dimer interface for class 3 BRAF mutations.

Altogether, our work complements the current understanding of kinase-impaired/kinase-dead BRAF mutations, while highlighting key biochemical properties of the most common kinase-dead mutation, BRAF^{D594G}. These results identify how BRAF^{D594G}:CRAF heterodimers sustain increased MEK/ERK activation in cancer cells, while exposing a new allosteric site, at the dimer interface, to target class 3 BRAF mutations.

Experimental procedures

Compounds and reagents

Dabrafenib, AZ-628, PLX-4720, PB, SB-590885, and dorsomorphin (compound C) 2HCl were purchased from Selleckchem. 10 mM inhibitor stocks were made in DMSO (RAF inhibitors)/double-distilled water ($AMPK_i$) and stored at −20 °C. [γ-^{32}P]ATP (#NEG002Z250UC) was purchased from PerkinElmer Life Sciences. Polyethyleneimine hydrochloride-MAX (PEI-MAX) was purchased from Polysciences (#24765). Fetal bovine serum was purchased from Gemini Bio-Products (#100-602). L-Glutamine (#25030-081), Dulbecco's modified Eagle's medium (DMEM, #11995-065), trypsin-EDTA (#25300-054), Opti-MEM (#31985-070), and PBS (#10010-023) were purchased from Gibco. SYPRO Orange dye (#S6651) was purchased from Invitrogen. Braftide was synthesized as described previously (28). All other reagents were purchased without further purification.

Antibodies

Anti-FLAG M2 mouse (#F1804), anti-FLAG M2 rabbit (#F2555), anti-FLAG M2 magnetic resin (#M8823), and pCRAF (pSer-338) antibody (#05-538) were purchased from Sigma–Aldrich. HA antibody (#26183) was purchased from Invitrogen. Profinity IMAC Ni charged resin (#156-0131) was purchased from Bio-Rad. Anti-p-MEK1/2 Ser-217/221 (#9154), anti-pERK1/2 (#4370), anti-BRAF (#14814), anti-CRAF (#9422), Raptor (#2280), and phospho-Raptor (#89146) were purchased from Cell Signaling. Actin antibody was purchased from Sigma (#A2228). Phospho-BRAF (pSer-729) antibody (#ab124794) was purchased from Abcam.

Plasmids

WT BRAF/6x-HIS/FLAG and CRAF/6x-HIS/HA were designed as described previously (15). BRAF-D594G/6x-HIS/FLAG, BRAF-D594GΔN-tail/FLAG, BRAF-D594GΔRBD/FLAG, BRAF-D594GΔCR2/FLAG, BRAF-D594GΔSSDD/FLAG, BRAF-S465D/S467D/6x-HIS/FLAG, and CRAF/FLAG/MBP were created using common cloning procedures with pCDNA^{TM} 4/TO (Invitrogen) as the vector. WT CD-BRAF with 16 mutations was a gift from Dr. Ronen Marmorstein's laboratory (42), and WT CD-BRAF (aa 442–723), with the SSDD motif added, was inserted into pET-21(+) vector (Sigma–Aldrich). CD-D594G/6x-HIS was generated using common cloning procedures with pET-21 + (Sigma–Aldrich) as the vector.

Cell lines

WM3629 and HTB177 were purchased from Rockland and HTCC, respectively. HEK293 cells were a gift from Dr. Catherine Moore (University of the Sciences).

CD-BRAF purification

CD-BRAF-6xHIS was transformed into BL21 codon plus *E. coli* cells and grown at 37 °C to an optical density of 600 nm of 0.6–0.8, and then 1 mM isopropyl 1-thio-β-D-galactopyranoside was added and the cells were induced at 16 °C with stirring at 200 rpm. The harvested pellet was resuspended in lysis buffer (50 mM HEPES buffer, pH 7.4, 250 mM NaCl, 50 mM KCl, 10 mM imidazole, 10 mM β-mercaptoethanol, 10% glycerol, and protease inhibitor tablet (Sigma, catalog no. 11836170001)) and then lysed with a sonicator. The lysed suspension was centrifuged to separate the clarified supernatant, and then the supernatant was applied to pre-equilibrated nickel resin and incubated with rotation at 4 °C for 1–2 h. After resin incubation, the superna-

tant/resin slurry was added to a gravity column and washed with wash buffer (50 mM HEPES, pH 7.4, 250 mM NaCl, 10 mM imidazole, and 10% glycerol). 50–250 mM imidazole was added into low-salt buffer (50 mM HEPES, pH 7.4, 250 mM NaCl, and 10% glycerol) to elute the protein, which was pooled and concentrated, using a Millipore concentrator (#UFC803024), before injecting onto size-exclusion chromatography (column: Superdex 200 10/300 GL; #28-9909-44). The corresponding peaks were analyzed with SDS-PAGE and then pooled, concentrated, and aliquoted. These aliquots were flash-frozen in liquid nitrogen and stored at −80 °C.

Analytical ultracentrifugation

The velocity AUC experiment was performed as described previously (42). Briefly, 10–15 μM WT CD-BRAF and CD-D594G were centrifuged at 42,000 r.p.m. for ∼8 h while data were collected over the entire time frame. The results were analyzed with SEDFIT to calculate the continuous *c*(*S*) distribution, and data were graphed using Origin.

Molecular dynamics simulations

The molecular dynamics simulations were performed as described previously (17). In brief, the crystal structures that were acquired from the respective PDB files were cleaned up and solvated in a periodic box using TIP3P water molecules. The ff14SB (43) force field was used on the proteins. GPU-implemented Amber18 was utilized for each MD simulation (44). All systems were equilibrated using the same protocol for solvent minimization, heating, and NPT simulation at 1 atmosphere and 300 K. Production runs using the NVT system at 300 K were then applied for 200–400 ns per system. The trajectories were then investigated with the cpptraj program in the Amber18 package for hydrogen bond interactions, distance, root mean square deviation, etc. as conveyed in the results sections describing Fig. 1, 2 and 4.

Transient transfection into mammalian cells

HEK293 cells were transiently transfected as described previously (17). In brief, 0.5–1 million HEK293 cells were plated onto 12- or 6-well plates, respectively, and then were incubated overnight until the cells reached 40–60% confluence. DNA (0.5–2 μg) was mixed with PEI-MAX in a 1:3 ratio. DNA:PEI-MAX was added to fresh DMEM on the HEK293 cells. The cells were washed with ice-cold PBS after 24–48 h and then lysed in 4% SDS. The harvested lysate was applied to homogenizer columns, and the flow-through protein concentration was analyzed using a BCA kit (Pierce, #23225). 10–40 μg of lysates were used for Western blotting analyses.

BRAF:CRAF co-immunoprecipitation

For immunoprecipitation, 5 million HEK293 cells were plated onto a 10-cm dish and incubated overnight at 37 °C with 5% CO_2. Once the cells reached a confluence of 40–60%, the DMEM was aspirated out, and fresh DMEM was added. A total of 10 μg of DNA (5 μg + 5 μg for co-transfections) was mixed with 30 μg of PEI-MAX for 25 min and then added to the plated cells for 48 h at 37 °C with 5% CO_2. For inhibitor treatment, the cells were washed with PBS, and then DMEM containing DMSO (0.5% final) or inhibitor was added to the cells and incubated for 1 h at 37 °C with 5% CO_2. Cells were washed again with ice-cold PBS and then lysed in 1 ml of lysis buffer (50 mM HEPES, pH 7.4, 150 mM NaCl, 0.1% Nonidet P-40 (IGEPAL630), 1 mM EDTA, 5% glycerol, 1 mM phenylmethylsulfonyl fluoride, 20 mM β-glycerolphosphate, 2.5 mM sodium pyrophosphate, and protease inhibitor) for 2 h with rotation at 4 °C. The lysate was clarified, and 0.5–1 mg of lysate was applied to 10 μl of pre-equilibrated amylose or FLAG resin for 2 h with rotation at 4 °C. The resin was washed 5× (5 min each wash) with lysis buffer and then resuspended in 2× dilution buffer (25 mM HEPES, pH 7.4, 0.125 mg/ml BSA, and 300 mM NaCl) for kinase assays or quenched with 4× loading dye to be analyzed by Western blotting.

Kinase-dead MEK1-K97M purification

Kinase-dead MEK1-K97M/6xHIS/GST protein was purified from BL21 codon plus *E. coli* as described previously (15). Briefly, the cells expressing MEK1 were harvested and then lysed in lysis buffer (20 mM HEPES, pH 7.4, 150 mM NaCl, 10 mM β-mercaptoethanol, Sigma–Aldrich Complete™ EDTA-free protease inhibitor tablets (product #11836170001), 5 mM imidazole, and 5% glycerol) with sonication (1 mg/ml lysozyme was used to help with lysis). The supernatant was added to equilibrated nickel resin and incubated for 2 h. The protein-bound resin was washed with low-salt buffer (20 mM HEPES, 150 mM NaCl, and 5% glycerol). MEK1 was eluted with elution buffer (150 mM imidazole, 20 mM HEPES, 150 mM NaCl, and 5% glycerol) and further purified, concentrated to >0.1 mg/ml, and stored as described above.

Western blotting– based kinase assay

The kinase assay was performed as described previously (17). In brief, the purified proteins or co-immunoprecipitation products were diluted with 2× dilution buffer and combined with 2× mixture buffer (25 mM HEPES, pH 7.4, 20 mM $MgCl_2$, 1 mM DTT, 50 mM β-glycerolphosphate, 0.2–2 μM MEK (0.1–1 μM final), and 2000 μM ATP) for 5–10 min, unless another time is indicated at 30 °C. The reaction was quenched using 4× loading dye and then analyzed by SDS-PAGE immunoblotting. The nitrocellulose membranes were probed with the suitable primary and secondary antibodies and imaged using fluorescence-based approaches on a GE Typhoon imager. Analyses of the immunoblots were analyzed using ImageJ software.

In-gel radioactive assay

As described previously (17), purified or co-immunoprecipitated proteins were mixed with a 2× mixture buffer (25 mM HEPES, pH 7.4, 20 mM $MgCl_2$, 50 mM β- glycerolphosphate, 1 mM DTT, 4 mM Na_3VO_4, 200 μM ATP, and 1 μCi of radioactive ATP). A final concentration of 1.3 μM MEK was added into the mixture buffer for tests that contained MEK and ATP. The reaction was incubated at 30 min at room temperature before being transferred to SDS-PAGE, dried, and imaged on a Typhoon imager.

Differential scanning fluorimetry

CD-D594G aliquots were diluted in DSF buffer (25 mM HEPES, pH 7.0, 150 mM NaCl) to a concentration of 5 μM

(final). To a 384-well PCR plate (Thermo Scientific, #AB-1384), 15 μl of CD-D594G, 4 μl of SYPRO Orange (5× final), and 1 μl of inhibitor in DMSO (25 μM final) were added. The plate was sealed with adhesive seal sheets (Thermo Scientific, #AB-1170) and then spun down and heated from 20 to 95 °C on QuantStudio 7 Flex (Applied Biosystems) with a ramp rate of 0.015 °C/s. The protein melt curves were produced, and the first derivative of the curve was used to analyze the data. The data were examined and plotted using Origin.

Cell viability

The cell viability assay was performed as described previously (28). In brief, WM3629 cells were plated onto a 96-well plate for 24 h before treatment. TAT-Braftide or AZ-628 were titrated on to the cells at the indicated concentrations for 48 or 96 h, respectively. The drug medium was switched out every 24 h, and then the WST reagent was added, in a 1:10 ratio, and incubated for 4 h at 37 °C. Absorbance readings were measured for the plate at 450 nm.

Author contributions—N. J. C., B. N., Z. L., M. Cavallo, A. Y. G., and M. Connolly data curation; N. J. C. and Z. W. formal analysis; N. J. C. validation; N. J. C. writing-original draft; Z. L. and Z. W. supervision; Z. L., A. Y. G., and Z. W. writing-review and editing; Z. W. funding acquisition; Z. W. methodology.

Acknowledgment—We thank the Marmorstein laboratory at the Perelman School of Medicine for help with biophysical experiments and for useful discussions.

References

1. Lavoie, H., and Therrien, M. (2015) Regulation of RAF protein kinases in ERK signalling. *Nat. Rev. Mol. Cell Biol.* **16,** 281–298 CrossRef Medline
2. Davies, H., Bignell, G. R., Cox, C., Stephens, P., Edkins, S., Clegg, S., Teague, J., Woffendin, H., Garnett, M. J., Bottomley, W., Davis, N., Dicks, E., Ewing, R., Floyd, Y., Gray, K., *et al.* (2002) Mutations of the BRAF gene in human cancer. *Nature* **417,** 949–954 CrossRef Medline
3. Yao, Z., Torres, N. M., Tao, A., Gao, Y., Luo, L., Li, Q., de Stanchina, E., Abdel-Wahab, O., Solit, D. B., Poulikakos, P. I., and Rosen, N. (2015) BRAF mutants evade ERK-dependent feedback by different mechanisms that determine their sensitivity to pharmacologic inhibition. *Cancer Cell* **28,** 370–383 CrossRef Medline
4. Karoulia, Z., Wu, Y., Ahmed, T. A., Xin, Q., Bollard, J., Krepler, C., Wu, X., Zhang, C., Bollag, G., Herlyn, M., Fagin, J. A., Lujambio, A., Gavathiotis, E., and Poulikakos, P. I. (2016) An integrated model of RAF inhibitor action predicts inhibitor activity against oncogenic BRAF signaling. *Cancer Cell* **30,** 485–498 CrossRef Medline
5. Poulikakos, P. I., Zhang, C., Bollag, G., Shokat, K. M., and Rosen, N. (2010) RAF inhibitors transactivate RAF dimers and ERK signalling in cells with wild-type BRAF. *Nature* **464,** 427–430 CrossRef Medline
6. Hatzivassiliou, G., Song, K., Yen, I., Brandhuber, B. J., Anderson, D. J., Alvarado, R., Ludlam, M. J. C., Stokoe, D., Gloor, S. L., Vigers, G., Morales, T., Aliagas, I., Liu, B., Sideris, S., Hoeflich, K. P., *et al.* (2010) RAF inhibitors prime wild-type RAF to activate the MAPK pathway and enhance growth. *Nature* **464,** 431–435 CrossRef Medline
7. Chang, M. T., Asthana, S., Gao, S. P., Lee, B. H., Chapman, J. S., Kandoth, C., Gao, J., Socci, N. D., Solit, D. B., Olshen, A. B., Schultz, N., and Taylor, B. S. (2016) Identifying recurrent mutations in cancer reveals widespread lineage diversity and mutational specificity. *Nat. Biotechnol.* **34,** 155–163 CrossRef Medline
8. Yao, Z., Yaeger, R., Rodrik-Outmezguine, V. S., Tao, A., Torres, N. M., Chang, M. T., Drosten, M., Zhao, H., Cecchi, F., Hembrough, T., Michels, J., Baumert, H., Miles, L., Campbell, N. M., de Stanchina, E., *et al.* (2017) Tumours with class 3 BRAF mutants are sensitive to the inhibition of activated RAS. *Nature* **548,** 234–238 CrossRef Medline
9. Nieto, P., Ambrogio, C., Esteban-Burgos, L., Gómez-López, G., Blasco, M. T., Yao, Z., Marais, R., Rosen, N., Chiarle, R., Pisano, D. G., Barbacid, M., and Santamaría, D. (2017) A Braf kinase-inactive mutant induces lung adenocarcinoma. *Nature* **548,** 239–243 CrossRef Medline
10. Joseph, E. W., Pratilas, C. A., Poulikakos, P. I., Tadi, M., Wang, W., Taylor, B. S., Halilovic, E., Persaud, Y., Xing, F., Viale, A., Tsai, J., Chapman, P. B., Bollag, G., Solit, D. B., and Rosen, N. (2010) The RAF inhibitor PLX4032 inhibits ERK signaling and tumor cell proliferation in a V600E BRAF-selective manner. *Proc. Natl. Acad. Sci. U.S.A.* **107,** 14903–14908 CrossRef Medline
11. Rajakulendran, T., Sahmi, M., Lefrançois, M., Sicheri, F., and Therrien, M. (2009) A dimerization-dependent mechanism drives RAF catalytic activation. *Nature* **461,** 542–545 CrossRef Medline
12. Heidorn, S. J., Milagre, C., Whittaker, S., Nourry, A., Niculescu-Duvas, I., Dhomen, N., Hussain, J., Reis-Filho, J. S., Springer, C. J., Pritchard, C., and Marais, R. (2010) Kinase-dead BRAF and oncogenic RAS cooperate to drive tumor progression through CRAF. *Cell* **140,** 209–221 CrossRef Medline
13. Grasso, M., Estrada, M. A., Berrios, K. N., Winkler, J. D., and Marmorstein, R. (2018) *N*-(7-Cyano-6-(4-fluoro-3-(2-(3-(trifluoromethyl)phenyl)acetamido)phenoxy)benzo[d]thiazol-2-yl)cyclopropanecarboxamide (TAK632) promotes inhibition of BRAF through the induction of inhibited dimers. *J. Med. Chem.* **61,** 5034–5046 CrossRef Medline
14. Thevakumaran, N., Lavoie, H., Critton, D. A., Tebben, A., Marinier, A., Sicheri, F., and Therrien, M. (2015) Crystal structure of a BRAF kinase domain monomer explains basis for allosteric regulation. *Nat. Struct. Mol. Biol.* **22,** 37–43 CrossRef Medline
15. Cope, N., Candelora, C., Wong, K., Kumar, S., Nan, H., Grasso, M., Novak, B., Li, Y., Marmorstein, R., and Wang, Z. (2018) Mechanism of BRAF activation through biochemical characterization of the recombinant full-length protein. *Chembiochem* **19,** 1988–1997 CrossRef Medline
16. Qin, J., Xie, P., Ventocilla, C., Zhou, G., Vultur, A., Chen, Q., Liu, Q., Herlyn, M., Winkler, J., and Marmorstein, R. (2012) Identification of a novel family of BRAF(V600E) inhibitors. *J. Med. Chem.* **55,** 5220–5230 CrossRef Medline
17. Cope, N., Novak, B., Candelora, C., Wong, K., Cavallo, M., Gunderwala, A., Liu, Z., Li, Y., and Wang, Z. (2019) Biochemical characterization of intact oncogenic BRAFV600E together with molecular dynamics simulations provide insight into the activation and inhibition mechanisms of RAF kinases. *Chembiochem* **20,** 2850–2861 CrossRef Medline
18. Weber, C. K., Slupsky, J. R., Kalmes, H. A., and Rapp, U. R. (2001) Active Ras induces heterodimerization of cRaf and BRaf. *Cancer Res.* **61,** 3595–3598 Medline
19. Chen, S. H., Zhang, Y., Van Horn, R. D., Yin, T., Buchanan, S., Yadav, V., Mochalkin, I., Wong, S. S., Yue, Y. G., Huber, L., Conti, I., Henry, J. R., Starling, J. J., Plowman, G. D., and Peng, S. B. (2016) Oncogenic BRAF deletions that function as homodimers and are sensitive to inhibition by RAF dimer inhibitor LY3009120. *Cancer Discov.* **6,** 300–315 CrossRef Medline
20. Freeman, A. K., Ritt, D. A., and Morrison, D. K. (2013) The importance of Raf dimerization in cell signaling. *Small GTPases* **4,** 180–185 CrossRef Medline
21. Yuan, J., Ng, W. H., Yap, J., Chia, B., Huang, X., Wang, M., and Hu, J. (2018) The AMPK inhibitor overcomes the paradoxical effect of RAF inhibitors through blocking phospho-Ser-621 in the C terminus of CRAF. *J. Biol. Chem.* **293,** 14276–14284 CrossRef Medline
22. Park, E., Rawson, S., Li, K., Kim, B. W., Ficarro, S. B., Pino, G. G., Sharif, H., Marto, J. A., Jeon, H., and Eck, M. J. (2019) Architecture of autoinhibited and active BRAF-MEK1–14-3-3 complexes. *Nature* **575,** 545–550 CrossRef Medline
23. Khazak, V., Astsaturov, I., Serebriiskii, I. G., and Golemis, E. A. (2007) Selective Raf inhibition in cancer therapy. *Expert Opin. Ther. Targets* **11,** 1587–1609 CrossRef Medline
24. Noeparast, A., Giron, P., De Brakeleer, S., Eggermont, C., De Ridder, U., Teugels, E., and De Grève, J. (2018) Type II RAF inhibitor causes superior

ERK pathway suppression compared to type I RAF inhibitor in cells expressing different BRAF mutant types recurrently found in lung cancer. *Oncotarget* **9,** 16110–16123 Medline

25. Zhang, C., Spevak, W., Zhang, Y., Burton, E. A., Ma, Y., Habets, G., Zhang, J., Lin, J., Ewing, T., Matusow, B., Tsang, G., Marimuthu, A., Cho, H., Wu, G., Wang, W., *et al.* (2015) RAF inhibitors that evade paradoxical MAPK pathway activation. *Nature* **526,** 583–586 CrossRef Medline
26. Holderfield, M., Merritt, H., Chan, J., Wallroth, M., Tandeske, L., Zhai, H., Tellew, J., Hardy, S., Hekmat-Nejad, M., Stuart, D. D., McCormick, F., and Nagel, T. E. (2013) RAF inhibitors activate the MAPK pathway by relieving inhibitory autophosphorylation. *Cancer Cell* **23,** 594–602 CrossRef Medline
27. Wang, Z., Yin, M., Chu, P., and Lou, M. (2019) STAT3 inhibitor sensitized KRAS-mutant lung cancers to RAF inhibitor by activating MEK/ERK signaling pathway. *Aging* **11,** 7187–7196 CrossRef Medline
28. Gunderwala, A. Y., Nimbvikar, A. A., Cope, N. J., Li, Z., and Wang, Z. (2019) Development of allosteric BRAF peptide inhibitors targeting the dimer interface of BRAF. *ACS Chem. Biol.* **14,** 1471–1480 CrossRef Medline
29. Jura, N., Shan, Y., Cao, X., Shaw, D. E., and Kuriyan, J. (2009) Structural analysis of the catalytically inactive kinase domain of the human EGF receptor 3. *Proc. Natl. Acad. Sci. U.S.A.* **106,** 21608–21613 CrossRef Medline
30. Hu, J., Stites, E. C., Yu, H., Germino, E. A., Meharena, H. S., Stork, P. J. S., Kornev, A. P., Taylor, S. S., and Shaw, A. S. (2013) Allosteric activation of functionally asymmetric RAF kinase dimers. *Cell* **154,** 1036–1046 CrossRef Medline
31. Shaw, A. S., Kornev, A. P., Hu, J., Ahuja, L. G., and Taylor, S. S. (2014) Kinases and pseudokinases: lessons from RAF. *Mol. Cell Biol.* **34,** 1538–1546 CrossRef Medline
32. Zeqiraj, E., Filippi, B. M., Goldie, S., Navratilova, I., Boudeau, J., Deak, M., Alessi, D. R., and van Aalten, D. M. (2009) ATP and MO25α regulate the conformational state of the STRADα pseudokinase and activation of the LKB1 tumour suppressor. *PLoS Biol.* **7,** e1000126 CrossRef Medline
33. Arteaga, C. L., Ramsey, T. T., Shawver, L. K., and Guyer, C. A. (1997) Unliganded epidermal growth factor receptor dimerization induced by direct interaction of quinazolines with the ATP binding site. *J. Biol. Chem.* **272,** 23247–23254 CrossRef Medline
34. Bandaranayake, R. M., Ungureanu, D., Shan, Y., Shaw, D. E., Silvennoinen, O., and Hubbard, S. R. (2012) Crystal structures of the JAK2 pseudokinase domain and the pathogenic mutant V617F. *Nat. Struct. Mol. Biol.* **19,** 754–759 CrossRef Medline
35. Hu, J., Yu, H., Kornev, A. P., Zhao, J., Filbert, E. L., Taylor, S. S., and Shaw, A. S. (2011) Mutation that blocks ATP binding creates a pseudokinase stabilizing the scaffolding function of kinase suppressor of Ras, CRAF and BRAF. *Proc. Natl. Acad. Sci. U.S.A.* **108,** 6067–6072 CrossRef Medline
36. Lemmon, M. A., Freed, D. M., Schlessinger, J., and Kiyatkin, A. (2016) The dark side of cell signaling: positive roles for negative regulators. *Cell* **164,** 1172–1184 CrossRef Medline
37. Wan, P. T. C., Garnett, M. J., Roe, S. M., Lee, S., Niculescu-Duvaz, D., Good, V. M., Project, C. G., Jones, C. M., Marshall, C. J., Springer, C. J., Barford, D., Marais, R., and Cancer Genome Project (2004) Mechanism of activation of the RAF-ERK signaling pathway by oncogenic mutations of B-RAF. *Cell* **116,** 855–867 CrossRef Medline
38. McClendon, C. L., Kornev, A. P., Gilson, M. K., and Taylor, S. S. (2014) Dynamic architecture of a protein kinase. *Proc. Natl. Acad. Sci. U.S.A.* **111,** E4623–E4631 CrossRef Medline
39. Carter, J., Tseng, L.-H., Zheng, G., Dudley, J., Illei, P., Gocke, C. D., Eshleman, J. R., and Lin, M.-T. (2015) Non-p.V600E BRAF mutations are common using a more sensitive and broad detection tool. *Am. J. Clin. Pathol.* **144,** 620–628 CrossRef Medline
40. Kondo, Y., Ognjenović, J., Banerjee, S., Karandur, D., Merk, A., Kulhanek, K., Wong, K., Roose, J. P., Subramaniam, S., and Kuriyan, J. (2019) Cryo-EM structure of a dimeric B-Raf:14-3-3 complex reveals asymmetry in the active sites of B-Raf kinases. *Science* **366,** 109–115 CrossRef Medline
41. Montagut, C., Sharma, S. V., Shioda, T., McDermott, U., Ulman, M., Ulkus, L. E., Dias-Santagata, D., Stubbs, H., Lee, D. Y., Singh, A., Drew, L., Haber, D. A., and Settleman, J. (2008) Elevated CRAF as a potential mechanism of acquired resistance to BRAF inhibition in melanoma. *Cancer Res.* **68,** 4853–4861 CrossRef Medline
42. Grasso, M., Estrada, M. A., Ventocilla, C., Samanta, M., Maksimoska, J., Villanueva, J., Winkler, J. D., and Marmorstein, R. (2016) Chemically linked Vemurafenib inhibitors promote an inactive BRAF(V600E) conformation. *ACS Chem. Biol.* **11,** 2876–2888 CrossRef Medline
43. Maier, J. A., Martinez, C., Kasavajhala, K., Wickstrom, L., Hauser, K. E., and Simmerling, C. (2015) ff14SB: improving the accuracy of protein side chain and backbone parameters from ff99SB. *J. Chem. Theory Comput.* **11,** 3696–3713 CrossRef Medline
44. Case, D., Betz, R., Cerutti, D. S., Cheatham, T., Darden, T., Duke, R., Giese, T. J., Gohlke, H., Götz, A., Homeyer, N., Izadi, S., Janowski, P., Kaus, J., Kovalenko, A., Lee, T.-S., *et al.* (2016). Amber 16, University of California, San Francisco CrossRef